Direct simulation of multiple scattering by discrete random media illuminated by Gaussian beams

Daniel W. Mackowski[1,*] and Michael I. Mishchenko[2]
[1]*Department of Mechanical Engineering, Auburn University, Alabama 36849, USA*
[2]*NASA Goddard Institute for Space Studies, 2880 Broadway, New York, New York 10025, USA*
(Received 3 November 2010; published 7 January 2011)

The conventional orientation-averaging procedure developed in the framework of the superposition *T*-matrix approach is generalized to include the case of illumination by a Gaussian beam (GB). The resulting computer code is parallelized and used to perform extensive numerically exact calculations of electromagnetic scattering by volumes of discrete random medium consisting of monodisperse spherical particles. The size parameters of the scattering volumes are 40, 50, and 60, while their packing density is fixed at 5%. We demonstrate that all scattering patterns observed in the far-field zone of a random multisphere target and their evolution with decreasing width of the incident GB can be interpreted in terms of idealized theoretical concepts such as forward-scattering interference, coherent backscattering (CB), and diffuse multiple scattering. It is shown that the increasing violation of electromagnetic reciprocity with decreasing GB width suppresses and eventually eradicates all observable manifestations of CB. This result supplements the previous demonstration of the effects of broken reciprocity in the case of magneto-optically active particles subjected to an external magnetic field.

DOI: 10.1103/PhysRevA.83.013804 PACS number(s): 42.25.Dd, 42.25.Bs, 42.25.Fx, 42.25.Kb

I. BACKGROUND AND MOTIVATION

In a wide range of scientific and engineering fields, the advancement of modern computational machinery and techniques has enabled the direct simulation of physical processes that, previously, could be predicted only by approximate or phenomenological methods. By direct simulation, we refer to a computation that accurately represents, at the smallest length and time scales that describe the system, the fundamental physical principles that govern the process. Some examples of such computations are the transient and three-dimensional numerical solution of the Navier-Stokes equations to a spatial resolution smaller than the Kolmogorov length scale (i.e., direct simulation of turbulent flows), the modeling of rarefied gas flows by Monte Carlo molecular dynamics methods, and the prediction of electromagnetic (EM) energy transport in discretely inhomogeneous media by a microlevel solution to the time-harmonic Maxwell equations. In all cases, the direct simulation can be viewed as a numerical experiment, in that the macroscopic-level properties generated from the simulations—which are typically obtained by time and/or spatial averaging over the microscopic-level calculation variables—can be viewed as an exact representation of the natural event.

The purpose of this paper is to present direct simulation results pertaining to the last example mentioned above: the transport of EM waves in particulate media. Specifically, we use the numerically exact superposition *T*-matrix method (STMM) to examine the scattering behavior of a macroscopic volume of discrete random medium. Our primary motivation in performing these calculations is to investigate phenomena that are inherently owing to multiple—as opposed to single—scattering, namely, diffuse radiative transfer (RT) and the effect of coherent backscattering (CB; otherwise known as weak localization of electromagnetic waves) [1–6]. These phenomena are of significant interest to a number of research fields, including biomedical and chemical diagnostics [7–10], Earth and planetary remote sensing [2], [11–14], heat transfer [15,16], and nanophotonics [17]. Therefore, a precise method of simulating these optical effects, for a set medium composition and type of illumination, will be an obvious benefit in solving inverse problems of predicting medium properties (particle size, composition, and concentration) from scattering measurement data.

Our previous simulations [18–20] (see also Refs. [21–23]) employed a computational model in which a set of spheres, randomly positioned within a spherical target volume, was excited with a monochromatic plane wave or a quasimonochromatic parallel beam of light of infinite lateral extent. For a sufficiently large number of spheres in the set, it was shown that configuration-averaged results, i.e., averaged over a large number of random realizations of the particle positions within the target volume, could be accurately represented by calculating the *T* matrix for a single realization and then performing an analytical orientation averaging of the scattering matrix values. It has been found that the numerically exact modeling of EM scattering by volumes of discrete random medium with packing densities exceeding 10% does reproduce—at least qualitatively—all basic RT and CB predictions, even though the asymptotic RT and CB theories refer to situations with negligibly small particle concentrations [5].

In the present work we employ the same basic strategy, except now the spherical target volume is excited with a Gaussian beam (GB) of varying width. Our practical rationale in adopting this approach is that the GB more accurately models the collimated sources (e.g., laser beams) that are used in many applications. On a more fundamental level, the GB provides an easily manipulated lateral length scale—the beam

*dmckwski@eng.auburn.edu

width—which can be used to test the microscopic theory of CB and, in particular, its interference premise rooted in the electromagnetic principle of reciprocity [24] coupled with the notion of cyclical diagrams [25,26]. It is well known that subjecting magneto-optically active particles to an external magnetic field is an efficient means of breaking reciprocity and suppressing the effect of CB [27,28]. In this respect, the use of GB can be envisioned as an alternative means of breaking reciprocity provided that the beam width is smaller than the size of the scattering volume or of the transport mean free path.

II. METHODS

A. Superposition *T*-matrix method with a Gaussian beam

We will describe briefly the key elements of the STMM solution procedure and the extension of analytical orientation averaging to Gaussian incident beams. The reader is referred to Refs. [29–31] for a detailed treatment of this numerically exact solver of the macroscopic Maxwell equations and the actual algorithm.

The solution procedure can be best described as an extension of the Lorenz-Mie theory to an ensemble of N_S neighboring spheres (Fig. 1). It is based upon the representation of the external ("ext") field as a superposition of the incident ("inc") and scattered ("sca") components, except in this case the scattered field consists of separate contributions radiated from each sphere, i.e.,

$$\mathbf{E}_{\rm ext}(\mathbf{r}) = \mathbf{E}_{\rm inc}(\mathbf{r}) + \mathbf{E}_{\rm sca}(\mathbf{r}) = \mathbf{E}_{\rm inc}(\mathbf{r}) + \sum_{i=1}^{N_S} \mathbf{E}_{{\rm sca},i}(\mathbf{r}), \quad (1)$$

where $\mathbf{E}$ is the electric field and $\mathbf{r}$ is the position vector. The scattered field contribution for each sphere is represented by an expansion of outgoing vector spherical wave functions (VSWFs), centered about the origin of the sphere. Likewise, the exciting field at each sphere, which will consist of the incident field plus the fields scattered from all other spheres in the ensemble, can be represented by an expansion of regular VSWF centered about the sphere origin. The transformation of an outgoing VSWF about one origin into an expansion of regular VSWF about a different origin—which is needed to formulate the scattering contribution to the exciting field—is accomplished by application of the addition theorem for VSWF [2]. Finally, the Lorenz-Mie theory provides the relation between the scattered and exciting field coefficients for each sphere. If each scattered field expansion is limited to L orders, the procedure results in a system of $2N_S L(L+2)$ linear interaction equations for the set of scattering coefficients, and the solution will be a function of the size parameters, refractive indices, and positions of all the spheres, and the characteristics of the incident field.

By application of the addition theorem to the individual sphere expansions, the scattered field from the ensemble can be described by a single outgoing VSWF expansion, centered about the common origin of the ensemble. The coefficients in this expansion will be linearly related to those for the incident field expansion, again centered about the ensemble origin, by the *T*-matrix relationship, i.e.,

$$a_{mnp} = \sum_{l=1}^{L_c} \sum_{k=-l}^{l} \sum_{q=1}^{2} T_{mnp\,klq}\, f_{klq}. \quad (2)$$

In the above, a and f denote the scattered and incident field expansion coefficients, respectively, while the triplet $\{m,n,p\}$ or $\{k,l,q\}$ denotes degree, order, and mode (1 for TM and 2 for TE) of the VSWF. The convergence order limit L_c for the T matrix will typically scale with the size parameter based on the smallest circumscribing sphere for the ensemble. The T matrix is most efficiently calculated from a sequence of solutions to the multiple-sphere interaction equations, with each solution corresponding to the degree–order–mode contribution to a unified VSWF expansion, centered about the cluster origin, of the incident field.

In the far-field zone of the multisphere group, one can define such useful quantities as the amplitude scattering matrix, the Stokes extinction matrix, the Stokes phase and scattering matrices, and the optical cross sections [32]. The random-orientation Stokes scattering matrix and optical cross sections can be obtained from analytical operations on the T matrix [30,31]. They are equally applicable to the cases of illumination with linearly and circularly polarized plane waves as well as quasimonochromatic parallel beams of infinite lateral extent.

Although the algorithm and code to perform the orientation averaging manipulations was originally developed for

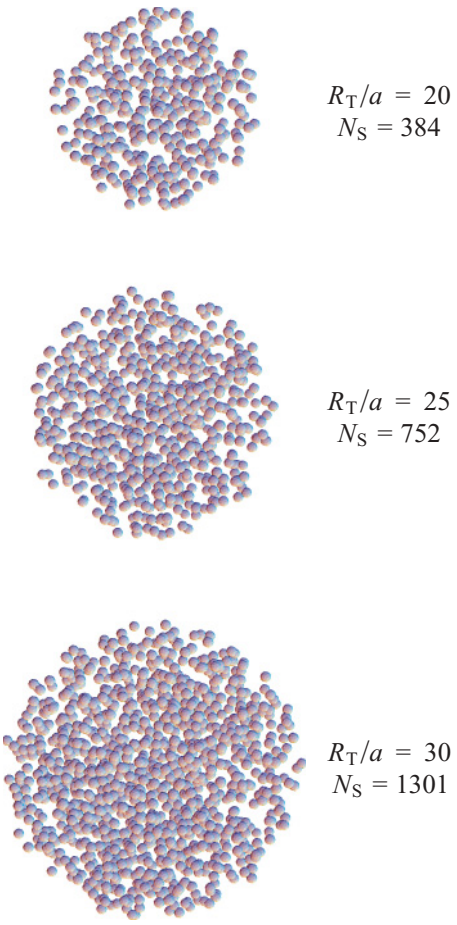

FIG. 1. (Color online) Multisphere targets.

plane-wave excitation [33], it turns out that it is relatively simple to modify the formulation to enable T-matrix orientation averaging for GB excitation, providing the focal point of the beam coincides with the origin of the ensemble. Taking for now a monochromatic GB [34,35], which propagates in the $+z$ direction and is polarized linearly in the x direction, the electric field distribution in the $z = 0$ plane is given by

$$\mathbf{E}_{\rm inc}(x,y,0) = \hat{\mathbf{x}} A \exp\left(-\frac{x^2+y^2}{\omega_0^2}\right), \tag{3}$$

in which A is a constant and ω_0 is the non-negative beam width parameter, i.e., the distance from the beam axis, in the $z = 0$ plane, required for the amplitude to decrease by a factor of $1/e$. As usual, we omit the time-harmonic factor $\exp(-i\omega t)$, where ω is the angular frequency, t is time, and $i = (-1)^{1/2}$.

The present application is concerned primarily with the propagation of a focused beam into a particulate medium. Accordingly, conditions are sought that minimize the spreading of the beam waist as a function of z. Such conditions will correspond to a relatively large $k\omega_0$, which is equivalent to a large diffraction-length/spot-size ratio $k\omega_0^2/\omega_0 = (2\pi\omega_0^2/\lambda)/\omega_0$, where k is the wave number in the host medium and λ is the respective wavelength. Such conditions also provide a simplified method for calculating the VSWF expansion coefficients for the GB: the localized approximation [36,37]. Specifically, if f_{mnp} denotes the expansion coefficients for a linearly polarized plane wave propagating in the direction (θ,φ) (defined with respect to the conventional right-handed spherical coordinate system) then the coefficients for the GB having the same polarization and propagation direction, denoted as f'_{mnp}, can be approximated for $k\omega_0 > 5$ by

$$f'_{mnp}(\theta,\varphi,k\omega_0) = f_{mnp}(\theta,\varphi)\bar{g}_n(k\omega_0), \tag{4}$$

in which

$$\bar{g}_n(k\omega_0) = \exp\left[-\left(\frac{n+1/2}{k\omega_0}\right)^2\right]. \tag{5}$$

Say now that T denotes the T matrix calculated for the multiparticle group. This matrix is independent of the incident field, but all random-orientation formulas of Refs. [30] and [31] have been derived by assuming a plane-wave illumination. Equation (4) then suggests that formulas for certain *scaled* quantities appearing in Ref. [31] are equally applicable to the case of GB, provided that T is replaced by the GB matrix T' calculated by the simple transformation of

$$T'_{mnp\,klq}(k\omega_0) = T_{mnp\,klq}\bar{g}_l(k\omega_0). \tag{6}$$

In other words, the scaled orientation-averaged properties of the ensemble, corresponding to a width $k\omega_0$ GB excitation, can then be obtained by substituting T' in the orientation-averaging formulas derived for plane-wave excitation. It is fundamentally important in this regard that the matrix T' defined by Eq. (6) satisfies the same rotation transformation rule as the original matrix T [2], [32]; this condition is met because the GB coefficients in Eq. (5) are azimuthal degree independent. The key point of this approach is that the calculation of the T matrix for a particular ensemble—which is the most time-consuming computational task—needs to be performed only once for a given cluster, and results for different $k\omega_0$ can be generated relatively quickly via the above transformation.

Examples of suitable scaled scattering characteristics involving elements of the Stokes scattering matrix S will be given below. The definition of other optical characteristics (e.g., the amplitude scattering matrix and the optical cross sections) is not unique, given the fact that the intensity of a GB is not uniform across the beam. We will avoid this uncertainty by displaying only appropriate scaled scattering characteristics. Note also that the concept of the Stokes scattering matrix is applicable to circularly as well as linearly polarized monochromatic GBs. It is also applicable to a quasimonochromatic GB having a phase rapidly fluctuating in the z direction. In this case one can think of partially polarized and even unpolarized GBs.

Calculations were performed by using an updated version of the multisphere T-matrix code described in Ref. [38]. The revised code is written in FORTRAN-90 in conjunction with message passing interface (MPI) instructions, and is designed to perform on distributed memory computer clusters. To test the code, we checked numerical convergence to the plane-wave results by selecting a large $k\omega_0$ value exceeding the size parameter of the multisphere target as well as by checking the equality of extinction and scattering efficiency factors in the case of nonabsorbing particles. In the latter case, the efficiency factors were found to agree to better than 10^{-12}.

B. Sphere target generation

The multisphere targets that were used in the calculations were generated by using a Monte Carlo algorithm designed to sequentially add spherical particles to a growing, enclosing spherical volume, in such a way so that (a) the spheres do not overlap, and (b) the distribution of spheres throughout the volume, at any point in the simulation, is statistically random with a uniform, set volume fraction.

The procedure is straightforward and is described as follows. Consider the simulation at a step N in the sequence, for which N spheres, each of radius a, are randomly distributed within a spherical volume of radius R_N. The sphere is considered to be inside the volume when its origin is enclosed by the volume. For a set volume fraction (packing density) f, the parameters R_N, a, and N are related by

$$N = f\left(\frac{R_N}{a}\right)^3. \tag{7}$$

At the next step $N + 1$ in the simulation the algorithm randomly samples a point $\mathbf{r}_{N+1}$ located within the annular volume formed between the R_{N+1} and R_N surfaces. The sampled point is accepted if a sphere placed at the point does not overlap with any of the N existing spheres. The maximum volume fraction that can be accommodated by this method is $\sim$0.5; in principle, the method would work in the limit of close packing ($f \to \sim$0.74), yet the number of samples required to find this condition would become computationally prohibitive. In addition, the method can break down for the initial values of N (i.e., 2–4) for sufficiently large f. In this case f is lowered until the method can start up, and f is raised to the set point once the algorithm becomes stable.

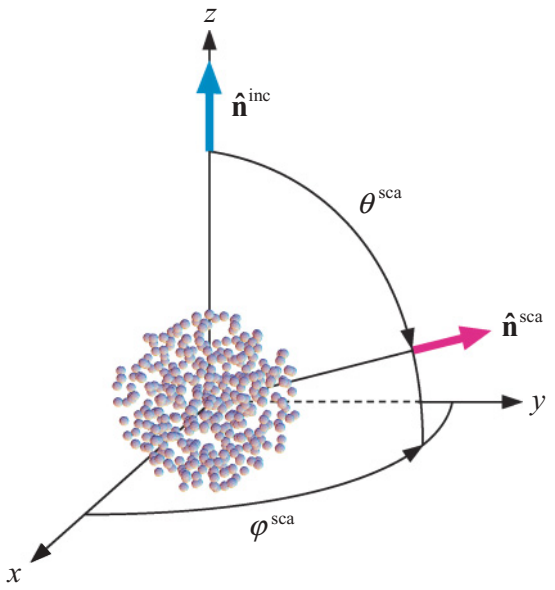

FIG. 2. (Color online) Scattering geometry.

Three multisphere targets were used in this study, corresponding to R_T/a ratios of 20, 25, and 30, where R_T is the radius of the enclosing sphere of the entire target. The sphere volume fraction was $f = 0.05$ for all three, and the associated N_S values for the targets were 384, 752, and 1301. Images of the clusters are shown in Fig. 1.

III. COMPUTER CALCULATIONS

The basic far-field scattering geometry is shown in Fig. 2. The incident light propagates along the positive z axis and is scattered in the direction of the unit vector $\hat{\mathbf{n}}^{\rm sca}$. The Stokes parameters I, Q, U, and V [32] of the incident and scattered light are specified with respect to the meridional plane of the scattering direction, and the transformation of the Stokes parameters upon scattering is described by the respective real-valued 4×4 Stokes scattering matrix S. Because the multisphere configurations shown in Fig. 1 are sufficiently "random" to begin with, averaging over all orientations of these configurations yields an azimuth-independent scattering matrix that is a function of only the scattering angle $\Theta = \theta^{\rm sca}$ and has only six independent significant elements:

$$\begin{bmatrix} I^{\rm sca} \\ Q^{\rm sca} \\ U^{\rm sca} \\ V^{\rm sca} \end{bmatrix} \propto \begin{bmatrix} S_{11}(\Theta) & S_{21}(\Theta) & 0 & 0 \\ S_{21}(\Theta) & S_{22}(\Theta) & 0 & 0 \\ 0 & 0 & S_{33}(\Theta) & S_{34}(\Theta) \\ 0 & 0 & -S_{34}(\Theta) & S_{44}(\Theta) \end{bmatrix} \begin{bmatrix} I^{\rm inc} \\ Q^{\rm inc} \\ U^{\rm inc} \\ V^{\rm inc} \end{bmatrix}. \tag{8}$$

In theory, the off-block diagonal terms are not identically zero; they would only be so if the multisphere configurations had a plane of symmetry [32]. We found, however, that in the cases considered, the maximum magnitude of the minor matrix elements is 0.001 that of the major elements.

The elements of the scattering matrix can be used to define specific optical observables corresponding to different types of polarization state of the incoming light [18,20]. For example, if the incident radiation is unpolarized, then the (1,1) element characterizes the angular distribution of the scattered intensity in the far-field zone of the target, while the ratio $-S_{21}(\Theta)/S_{11}(\Theta)$ gives the corresponding angular distribution of the degree of linear polarization. If the incident radiation is polarized linearly in the scattering plane, then the angular distribution of the cross-polarized scattered intensity is given by $\frac{1}{2}[S_{11}(\Theta) - S_{22}(\Theta)]$. Finally, if the incident radiation is polarized circularly in the counterclockwise direction when looking in the direction of propagation, then the circular polarization ratio is defined as the ratio of the same-helicity to the opposite-helicity scattered intensities: $\mu_C = [S_{11}(\Theta) + S_{44}(\Theta)]/[S_{11}(\Theta) - S_{44}(\Theta)]$.

All calculations used a fixed sphere size parameter of $x_S = ka = 2$ and relative refractive indices $m = 1.31$ or $m = 1.31 + i0.2$; this particular condition was chosen because the single-sphere polarization has an extended "shelf" of near-zero values at backscattering angles, thereby making it straightforward to isolate the polarization opposition effect (POE) caused by CB [20], [39].

The size parameters of the 384, 752, and 1301 sphere target volumes were $x_T = kR_T = 40, 50$, and 60. Four Lorenz-Mie orders were used to represent the individual-sphere scattered fields. For the $N_S = 1301$ target, the multiple-sphere interaction equations contained 62 448 unknowns, and the computation of the T matrix, to a converged order of $L_c = 67$, required solution of the interaction equations for 9246 right-hand sides. The code was parallel executed on 60 processors, and computation of the $N_S = 1301$ T matrix required over 5 days of run time. Once the T matrix was calculated and stored on file, computation of the random-orientation scattering matrix required 1 or 2 min for each incident beam state.

We performed computations for the three cluster targets (Fig. 1) and six incident beam conditions for each target, corresponding to a plane electromagnetic wave as well as GBs with $k\omega_0 = 10$, 20, 35, 50, and 100. The results of our computations are presented and discussed in the following section. The curves for $k\omega_0 = 100$ are virtually indistinguishable from those for plane-wave excitation and are not displayed.

IV. DISCUSSION

All data discussed in this section are the output of a direct numerically exact computer solution of the frequency-domain macroscopic Maxwell equations. As such, they include all the relevant physics by definition and require no physical *explanation*. However, it would be quite instructive to *interpret* them in terms of idealized, qualitative physical concepts such as forward-scattering interference, diffuse multiple scattering, and CB [18,19,40–42]. Doing so would accomplish two important objectives [43,44]. First, one would gain additional confidence in these numerical data by verifying whether they are generally consistent with the existing qualitative understanding of the underlying physics. Second, the above idealized physical concepts are valid, strictly speaking, only in the limit of vanishingly small packing density. Therefore, by analyzing numerically exact solutions of the Maxwell equations, one can gain further insight into the qualitative and even quantitative applicability of these concepts to discrete

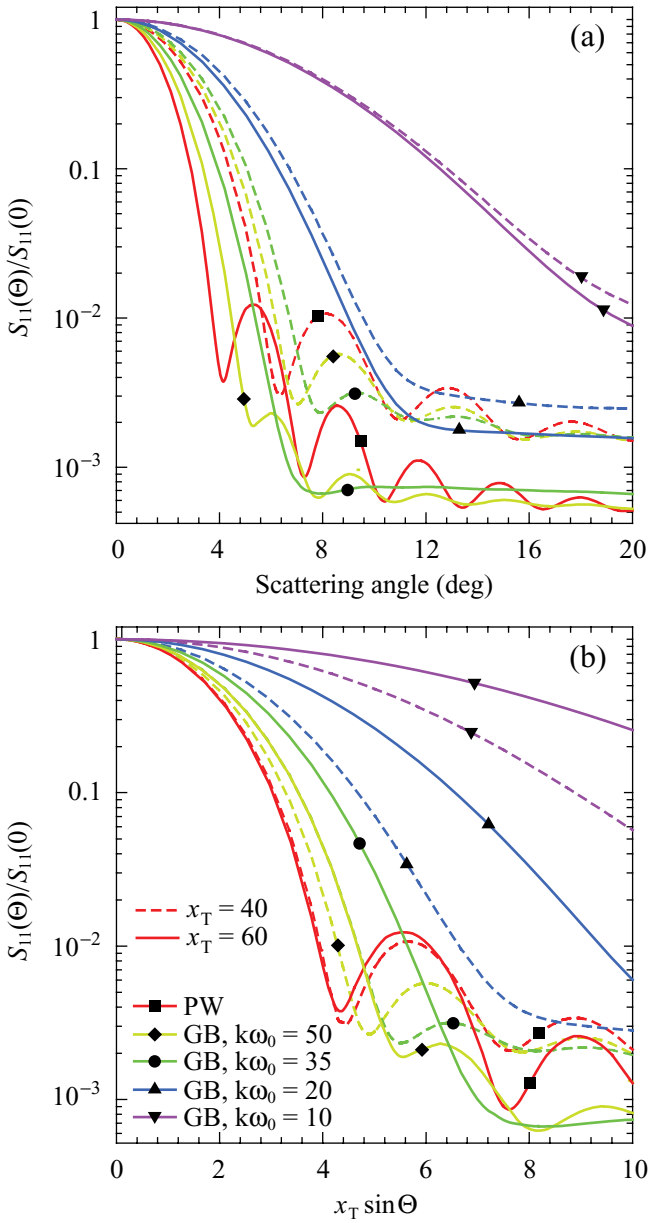

FIG. 3. (Color online) Scaled forward-scattering phase function vs (a) scattering angle and (b) scattering vector for plane-wave (PW) and Gaussian-beam (GB) illumination. Target size parameter $x_T = 60$ (solid curves) and 40 (dashed curves).

random media with packing densities deviating from zero significantly.

Shown in Fig. 3 are values of the scaled phase function $S_{11}(\Theta)/S_{11}(0)$ as a function of the scattering angle Θ (upper panel) and the dimensionless so-called scattering vector $q = x_T \sin\Theta$ (bottom panel) for scattering near the forward direction. The upper panel shows that the forward-scattering pattern is, as expected, controlled by forward-scattering interference [18], with the characteristic interference base length being the smaller of x_T or $k\omega_0$.

The nature of this effect in the case of plane-wave illumination is explained in Fig. 4(a), which demonstrates that the phases and amplitudes of the wavelets single scattered by different particles in the exact forward direction are the

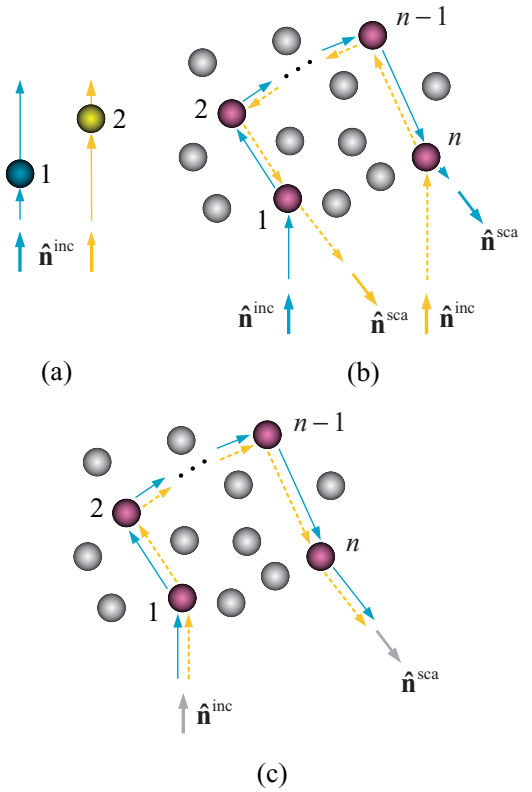

FIG. 4. (Color online) (a) Forward-scattering interference. (b) Interference origin of coherent backscattering. (c) Interference origin of the diffuse background.

same, irrespective of the particle positions. Therefore, all the wavelets interfere constructively, thereby resulting in a pronounced and narrow intensity peak centered at $\Theta = 0$. According to Ref. [45], the angular profiles of the forward-scattering peaks for all three targets should be almost the same if plotted versus the scattering vector q. Figure 3(b) shows that this theoretical prediction works very well up to $q \approx 6.5$.

In the case of GBs with widths smaller than the target size parameter, the phases and amplitudes of the forward-scattered wavelets change with particle positions because both the amplitude and the phase of the GB vary across the beam. As a consequence, the amplitude of the forward-scattering intensity peak can be expected to decrease and its angular width can be expected to increase. Indeed, let us consider for simplicity a two-sphere target and assume that the resulting "scalar" electric fields of the two forward-scattered wavelets at the far-field observation point are $E_1 \cos\omega t$ and $E_2 \cos(\omega t + \delta)$, respectively. Then the time-averaged total intensity in the exact forward direction is given by $(E_1^2 + E_2^2)\langle\cos^2 \omega t\rangle_t + \langle 2E_1E_2 \cos\omega t \cos(\omega t + \delta)\rangle_t = (E_1^2 + E_2^2)/2 + E_1E_2 \cos\delta$. If $E_1 = E_2$ and $\delta = 0$, which implies a plane incident wave, then the forward-scattering interference doubles the intensity. If, on the other hand, $E_1 \neq E_2$ owing to amplitude nonuniformity across the incident GB and/or $\delta \neq 0$ owing to phase nonuniformity across the beam, then $E_1E_2 \cos\delta < (E_1^2 + E_2^2)/2$, which implies a reduced amplitude of the forward-scattering intensity peak. This suppression is especially pronounced for widely separated particles with longer interference bases. Therefore, the

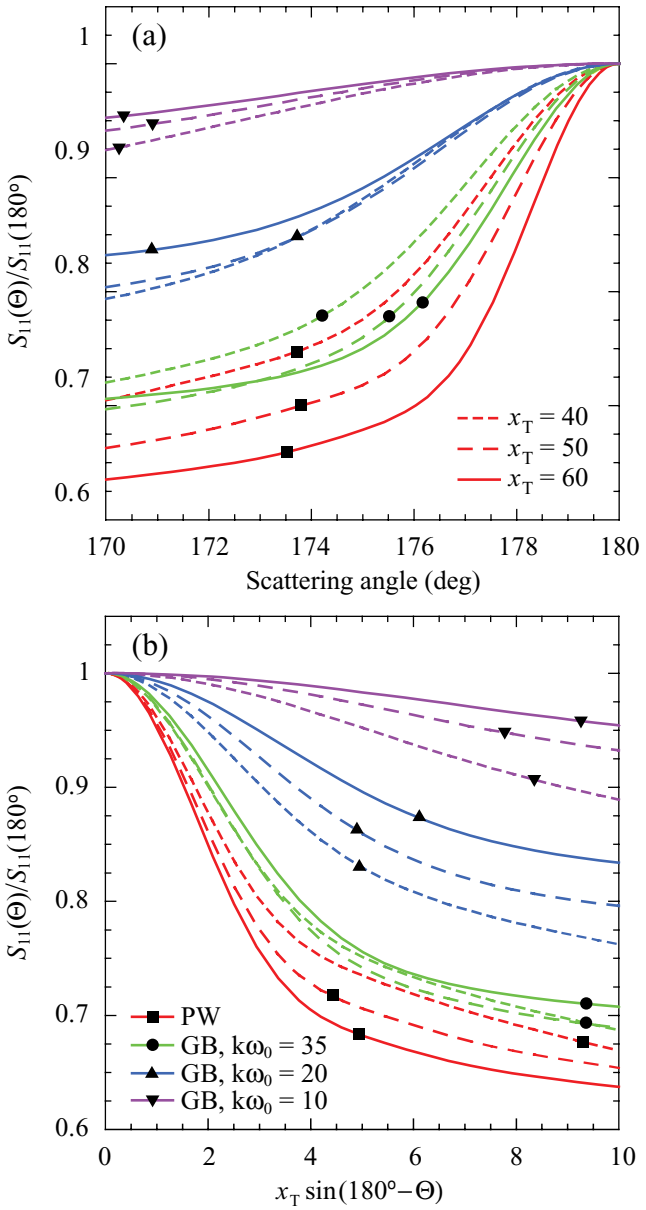

FIG. 5. (Color online) Scaled backscattering phase function vs (a) scattering angle and (b) scattering vector for plane-wave (PW) and Gaussian-beam (GB) illumination. Target size parameter $x_T = 60$ (solid curves), 50 (long-dashed curves), and 40 (short-dashed curves).

angular width of the forward-scattering intensity peak for a multiparticle target should increase with decreasing GB width and eventually become independent of the target size.

These qualitative predictions are fully corroborated by the results shown in Fig. 3. Indeed, one can easily recognize the strong suppressing effect of decreasing beam width on the amplitude of the forward-scattering intensity peak. Furthermore, the beams with widths $k\omega_0 = 10$ and 20 are intercepted entirely by the three multisphere targets; the forward-scattering pattern for these two widths is nearly independent of the target size and depends only on the beam width (upper panel). Likewise, all three clusters are entirely illuminated by the $k\omega_0 = 100$ GB (not shown) and the plane wave; the resulting scattering patterns are mostly independent of the beam width and depend solely on the cluster size parameter and, thus, on q (bottom panel).

Similar behavior is observed for the backscattering intensity peak in the case of unpolarized incident light. Shown in Fig. 5 are plots of $S_{11}(\Theta)/S_{11}(180^\circ)$ as a function of Θ (upper panel) and $q' = x_T \sin(180^\circ - \Theta)$ (bottom panel) for angles near the backward direction. These results can be interpreted in terms of the CB effect caused by constructive interference of conjugate wavelets propagating along the same multiparticle sequence but in opposite directions [Fig. 4(b)] [2–6]. Now, however, there can be an intricate convolution of three interference length scales: x_T, $k\omega_0$, and the transport mean free path.

The CB peak diminishes and widens for GBs with decreasing $k\omega_0$, which is an expected consequence of broken reciprocity. Indeed, let us consider two conjugate n-particle scattering paths, such as those in Fig. 4(b), with the resulting "scalar" electric fields at the observation point $E_1 \cos \omega t$ for the path starting at particle 1 and $E_2 \cos(\omega t + \delta)$ for the path starting at particle n. Their time-averaged contribution to the total diffuse intensity in the exact backscattering direction is $I_D = (E_1^2 + E_2^2)\langle \cos^2 \omega t \rangle_t = (E_1^2 + E_2^2)/2$, while their contribution to the coherent intensity is $\langle 2E_1E_2 \cos \omega t \cos(\omega t + \delta)\rangle_t = E_1E_2 \cos \delta \leqslant I_D$. The inequality occurs if $E_1 \neq E_2$ (as a consequence of amplitude nonuniformity across the incident GB) and/or if $\delta \neq 0$ (owing to phase nonuniformity across the incident beam). The equality occurs only if $E_1 = E_2$ and $\delta = 0$, implying a plane electromagnetic wave and, thus, full reciprocity. Again, the suppression of the CB maximum is especially pronounced for multiparticle sequences with widely separated end members and, thus, with long interference bases. Therefore, the angular width of the CB intensity peak increases with decreasing GB width.

Because the likely effects of absorption on CB via the suppression of multiple scattering and reduction of the

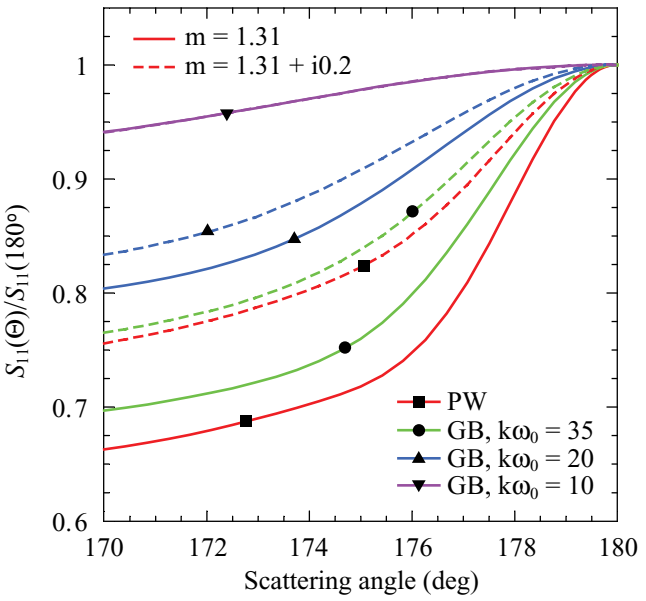

FIG. 6. (Color online) Scaled backscattering phase function vs scattering angle for plane-wave (PW) and Gaussian-beam (GB) illumination. Target size parameter $x_T = 50$. Particle refractive indices $m = 1.31$ (solid curves) and $1.31 + i0.2$ (dashed curves).

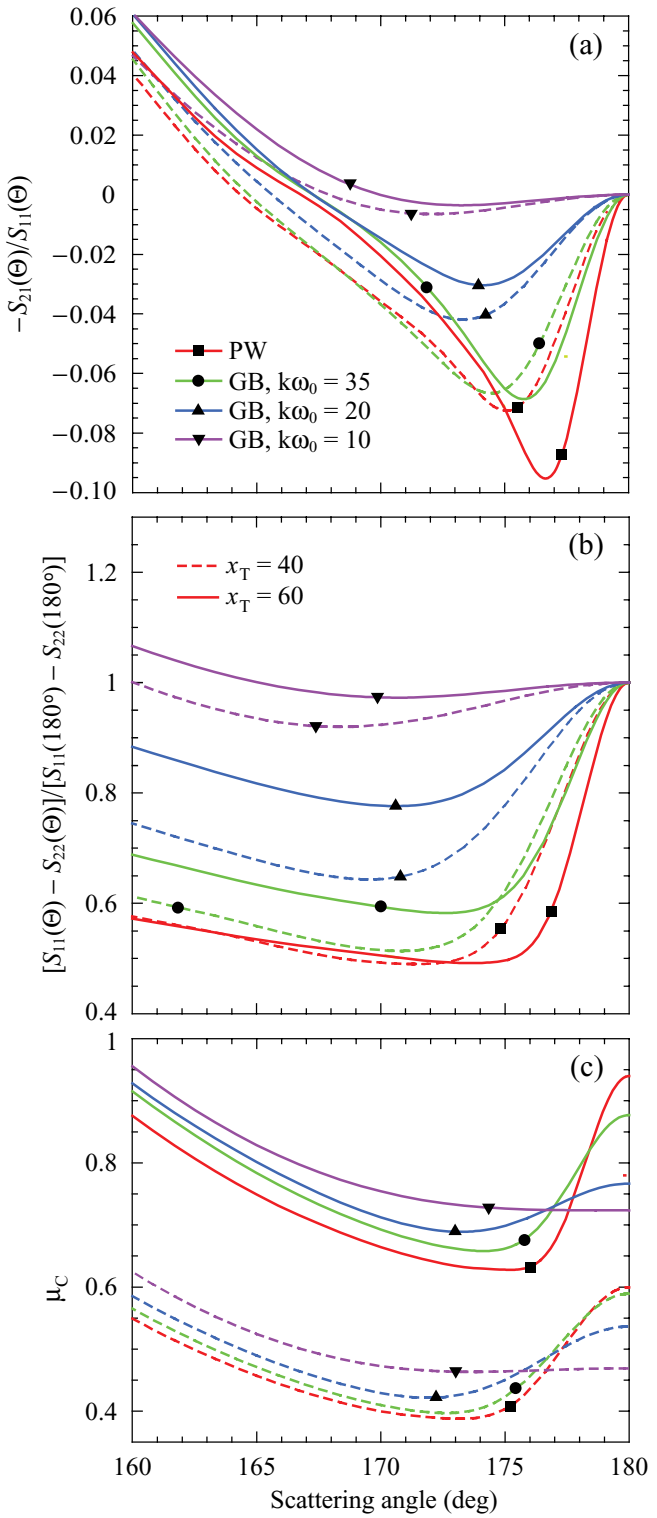

FIG. 7. (Color online) (a) Linear polarization, (b) scaled cross-polarized scattered intensity, and (c) circular polarization ratio vs scattering angle. Target size parameter $x_T = 60$ (solid curves) and 40 (dashed curves).

transport mean free path are well documented [46], it is interesting to compare the results of T-matrix computations for nonabsorbing and absorbing particles (Fig. 6). As expected, nonzero absorption serves to decrease the amplitudes of the CB intensity peaks and make them wider. Not surprisingly, however, the differences between the respective solid and dashed curves in Fig. 6 decrease with decreasing $k\omega_0$ and become negligibly small for $k\omega_0 = 10$, i.e., when the beam width is small enough to eradicate the CB peak entirely.

The effects of decreasing $k\omega_0$ on the POE caused by CB in the case of unpolarized incident light [20,39] are also quite consistent with the above discussion. With decreasing beam width, the depth of the POE decreases and its width increases [see Fig. 7(a)]. Other backscattering features observable with linearly and circularly polarized incident light also evolve with increasing $k\omega_0$, as expected and in agreement with their CB origin [see Figs. 7(b) and 7(c)].

Unlike the cyclical diagrams exemplified by Fig. 4(b), the ladder diagrams, such as the one shown in Fig. 4(c), can be expected to be much less affected by the lateral nonuniformity of a GB because in this case the entrance points for both interfering wavelets are the same. Figure 8 is fully consistent

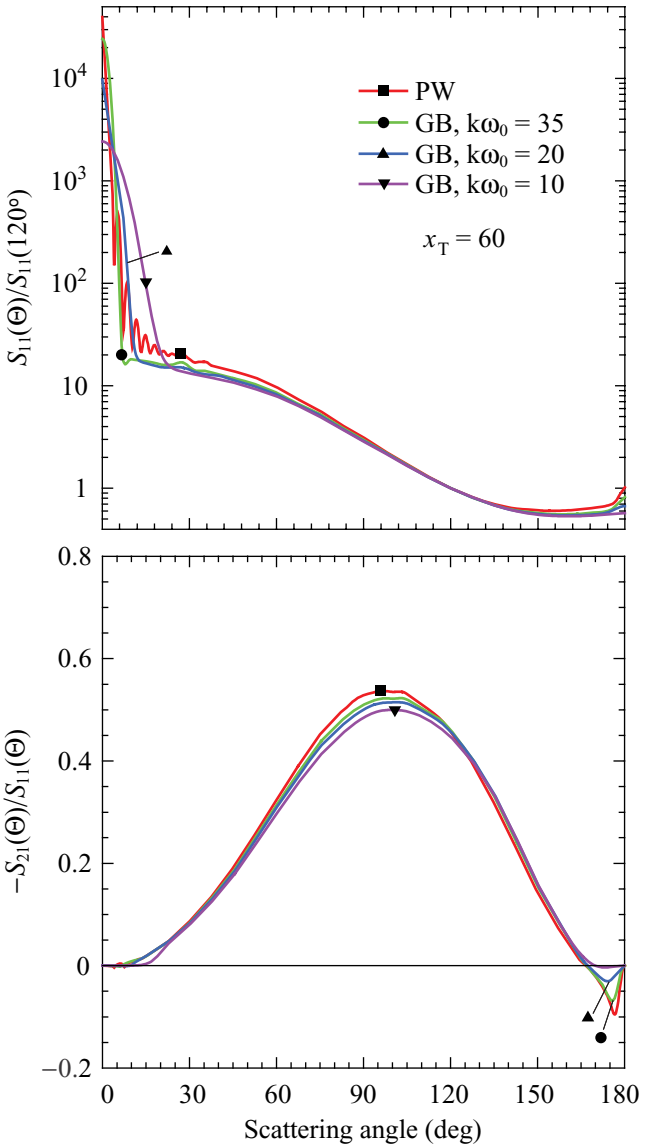

FIG. 8. (Color online) Scaled phase function and linear polarization vs scattering angle for plane-wave (PW) and Gaussian-beam (GB) illumination. Target size parameter $x_T = 60$.

with this assessment. In fact, it is quite remarkable that decreasing $k\omega_0$ eventually eradicates all manifestations of CB and strongly suppresses the forward-scattering interference while doing virtually nothing to the angular profiles of intensity and polarization at intermediate scattering angles.

V. CONCLUDING REMARKS

The important advantages of the direct computer simulation of electromagnetic scattering by a volume of discrete random media are that it (a) includes by definition all the relevant physics, (b) yields numerical results with known and guaranteed accuracy, (c) does not require the asymptotic assumption of a very small volume fraction, and (d) allows one to vary all physical parameters of the scattering target one at a time.

As we have demonstrated above, this approach can be used also to simulate a variety of illumination conditions differing from the standard plane-wave incidence, the objectives being an improved modeling of existing light sources and the verification of expected consequences of broken reciprocity.

Based on our numerical data and discussion, we can conclude that all scattering patterns observed in the far-field zone of a volume of discrete random medium and their evolution with decreasing width of the incident Gaussian beam can be interpreted in terms of such simplified concepts as forward-scattering interference, CB, and diffuse multiple scattering. In particular, the increasing violation of electromagnetic reciprocity with decreasing beam width serves to suppress and eventually eradicate all observable manifestations of CB. This result is an important supplement to the previous demonstration of the effects of broken reciprocity in the case of magneto-optically active particles subjected to an external magnetic field [27,28].

Our numerically exact data demonstrate again the qualitative (if not semiquantitative) applicability of the idealized notions of forward-scattering interference, CB, and diffuse multiple scattering in situations when particles forming the scattering volume are not always in the far-field zones of each other (cf. [18–20,23,47]). An important corollary of this result is that the domain of practical applicability of the classical theories of RT and CB may be wider than that implied by the formal microphysical derivation of these theories from the macroscopic Maxwell equations [5]. Should this corollary be further substantiated and quantified, its importance to the various applied-science and engineering disciplines would be impossible to overstate (cf. Refs. [7–16,48–51]).

ACKNOWLEDGMENT

This research was supported in part by the NASA Radiation Sciences.

[1] S. Chandrasekhar, *Radiative Transfer* (Oxford University Press, Oxford, 1950).
[2] L. Tsang, J. A. Kong, and R. T. Shin, *Theory of Microwave Remote Sensing* (Wiley, New York, 1985).
[3] Yu. N. Barabanenkov, Yu. A. Kravtsov, V. D. Ozrin, and A. Saichev, Prog. Opt. **29**, 65 (1991).
[4] *Wave Scattering in Complex Media: From Theory to Applications*, edited by B. van Tiggelen and S. E. Skipetrov (Kluwer, Dordrecht, The Netherlands, 2003).
[5] M. I. Mishchenko, L. D. Travis, and A. A. Lacis, *Multiple Scattering of Light by Particles: Radiative Transfer and Coherent Backscattering* (Cambridge University Press, Cambridge, 2006).
[6] E. Akkermans and G. Montambaux, *Mesoscopic Physics of Electrons and Photons* (Cambridge University Press, Cambridge, 2007).
[7] *Scattering in Polymetric and Colloidal Systems*, edited by W. Brown and K. Mortensen (Gordon and Breach, Amsterdam, 2000).
[8] V. V. Tuchin, L. V. Wang, and D. A. Zimnyakov, *Optical Polarization in Biomedical Applications* (Springer, Berlin, 2006).
[9] V. Tuchin, *Tissue Optics* (SPIE, Bellingham, WA, 2007).
[10] J. Liu, Z. Xu, Q. Song, R. L. Konger, and Y. L. Kim, J. Biomed. Opt. **15**, 037011 (2010).
[11] G. L. Stephens, *Remote Sensing of the Lower Atmosphere* (Oxford University Press, New York, 1994).
[12] J. W. Hovenier, C. van der Mee, and H. Domke, *Transfer of Polarized Light in Planetary Atmospheres* (Kluwer, Dordrecht, 2004).
[13] *Photpolarimetry in Remote Sensing*, edited by G. Videen, Ya. Yatskiv, and M. Mishchenko (Kluwer, Dordrecht, 2004).
[14] M. I. Mishchenko, V. K. Rosenbush, N. N. Kiselev, D. F. Lupishko, V. P. Tishkovets, V. G. Kaydash, I. N. Belskaya, Y. S. Efimov, and N. M. Shakhovskoy, *Polarimetric Remote Sensing of Solar System Objects* (Akademperiodyka, Kyiv, 2010).
[15] M. Kaviany, *Heat Transfer Physics* (Cambridge University Press, Cambridge, 2008).
[16] J. R. Howell, R. Siegel, and M. P. Mengüç, *Thermal Radiation Heat Transfer* (CRC, Boca Raton, FL, 2010).
[17] S. V. Gaponenko, *Introduction to Nanophotonics* (Cambridge University Press, Cambridge, 2010).
[18] M. I. Mishchenko, L. Liu, D. W. Mackowski, B. Cairns, and G. Videen, Opt. Express **15**, 2822 (2007).
[19] M. I. Mishchenko, J. M. Dlugach, and L. Liu, Phys. Rev. A **80**, 053824 (2009).
[20] M. I. Mishchenko, J. M. Dlugach, L. Liu, V. K. Rosenbush, N. N. Kiselev, and Yu. G. Shkuratov, Astrophys. J. **705**, L118 (2009).
[21] S. Tseng, Opt. Commun. **281**, 1986 (2008).
[22] Y. Okada and A. A. Kokhanovsky, J. Quant. Spectrosc. Radiat. Transfer **110**, 902 (2009).
[23] F. Voit, J. Schäfer, and A. Kienle, Opt. Lett. **34**, 2593 (2009).
[24] D. S. Saxon, Phys. Rev. **100**, 1771 (1955).
[25] Yu. N. Gnedin and A. Z. Dolginov, Sov. Phys. JETP **18**, 784 (1964).
[26] Yu. N. Barabanenkov, Radiophys. Quant. Electron. **16**, 65 (1973).
[27] F. C. MacKintosh and S. John, Phys. Rev. B **37**, 1884 (1988).
[28] F. A. Erbacher, R. Lenke, and G. Maret, Europhys. Lett. **21**, 551 (1993).

[29] B. Peterson, and S. Ström, Phys. Rev. D **8**, 3661 (1973).
[30] D. W. Mackowski, J. Opt. Soc. Am. A **11**, 2851 (1994).
[31] D. W. Mackowski and M. I. Mishchenko, J. Opt. Soc. Am. A **13**, 2266 (1996).
[32] M. I. Mishchenko, L. D. Travis, and A. A. Lacis, *Scattering, Absorption, and Emission of Light by Small Particles* (Cambridge University Press, Cambridge, 2002), [http://www.giss.nasa.gov/staff/mmishchenko/books.html].
[33] [ftp://ftp.eng.auburn.edu/pub/dmckwski/scatcodes/index.html].
[34] L. Mandel and E. Wolf, *Optical Coherence and Quantum Optics* (Cambridge University Press, Cambridge, 1995), Sec. 5.6.2.
[35] K. E. Oughstun, *Electromagnetic and Optical Pulse Propagation* (Springer, Berlin, 2009), Vol. 2, Sec. 9.4.1.
[36] A. Doicu and T. Wriedt, Appl. Opt. **36**, 2971 (1997).
[37] A. Doicu and T. Wriedt, Opt. Commun. **136**, 114 (1997).
[38] D. W. Mackowski, J. Quant. Spectrosc. Radiat. Transfer (in press).
[39] M. I. Mishchenko, J.-M. Luck, and Th. M. Nieuwenhuizen, J. Opt. Soc. Am. A **17**, 888 (2000).
[40] A. P. Ivanov and A. Ya. Khairullina, Opt. Spectrosc. **23**, 83 (1967).
[41] A. P. Ivanov, A. Ya. Khairullina, and T. N. Kharkova, Opt. Spectrosc. **28**, 204 (1970).
[42] K. Muinonen, Waves Random Media **14**, 365 (2004).
[43] V. P. Tishkovets and M. I. Mishchenko, J. Quant. Spectrosc. Radiat. Transfer **111**, 645 (2010).
[44] M. I. Mishchenko, V. P. Tishkovets, L. D. Travis, B. Cairns, J. M. Dlugach, L. Liu, V. K. Rosenbush, and N. N. Kiselev, J. Quant. Spectrosc. Radiat. Transfer (in press).
[45] M. I. Mishchenko, J. W. Hovenier, and D. W. Mackowski, J. Opt. Soc. Am. A **21**, 71 (2004).
[46] S. Etemad, R. Thompson, M. J. Andrejco, S. John, and F. C. MacKintosh, Phys. Rev. Lett. **59**, 1420 (1987).
[47] K. Muinonen and E. Zubko, in *Proceedings of the Conference on Electromagnetic and Light Scattering XII*, edited by K. Muinonen, A. Penttilä, H. Lindqvist, T. Nousiainen, and G. Videen (University of Helsinki, Helsinki, 2010), p. 194.
[48] Yu. G. Shkuratov, K. Muinonen, E. Bowell, K. Lumme, J. I. Peltoniemi, M. A. Kreslavsky, D. G. Stankevich, V. P. Tishkovets, N. V. Opanasenko, and L. Y. Melkumova, Earth, Moon, Planets **65**, 201 (1994).
[49] V. K. Rosenbush, V. A. Avramchuk, A. E. Rosenbush, and M. I. Mishchenko, Astrophys. J. **487**, 402 (1997).
[50] V. Rosenbush, N. Kiselev, and V. Avramchuk, J. Quant. Spectrosc. Radiat. Transfer **100**, 325 (2006).
[51] N. Kiselev, V. Rosenbush, F. Velichko, and S. Zaitsev, J. Quant. Spectrosc. Radiat. Transfer **110**, 1713 (2009).